Studies of transitions in ordered and disordered perovskites: X-ray and Mossbauer scattering experiments

1991 J. Phys.: Condens. Matter 3 4173

(http://iopscience.iop.org/0953-8984/3/23/006)

J. Phys.: Condens. Matter 3 (1991) 4173–4185. Printed in the UK

Studies of transitions in ordered and disordered perovskites: x-ray and Mössbauer scattering experiments

C N W Darlington
School of Physics and Space Research, University of Birmingham, Birmingham B15 2TT, UK

Received 30 October 1990, in final form 5 March 1991

Abstract. Scattering experiments using Mössbauer gamma rays and x-rays have been performed on ordered and disordered $Pb(Sc_{0.5}Nb_{0.5})O_3$ (PSN), and $Pb(Fe_{0.5}Nb_{0.5})O_3$ (PFN) which exists only in a disordered state. All three materials are ferroelectric at room temperature and undergo a change to a paraelectric form close to 100 °C.

No evidence of an increase in inelastic scattering was found as the transition was approached in any of the materials studied. Rather large differences were found in the magnitude of Debye–Waller factors calculated from integrated intensities obtained using x-rays and Mössbauer gamma rays. These differences arise because part of the atomic displacement from positions of high symmetry is dynamic.

1. Introduction

The effect of chemical disorder on the transitions and properties of $Pb(Sc_{0.5}Nb_{0.5})O_3$ (PSN), and $Pb(Sc_{0.5}Ta_{0.5})O_3$ (PST), has been the subject of many studies [1–7]. The transition to the ferroelectric form in the disordered materials is broad. Order in the arrangement of the Sc and Nb or Ta ions can be induced by annealing at temperatures around 950–1000 °C [1, 2]. For relatively short anneal times the order is inhomogeneous, with ordered domains existing in a disordered matrix, resulting in the transition to the ferroelectric state occurring at two different temperatures. As the anneal time is increased, true long-range order sets in, and only a sharp transition to the ferroelectric form remains. In PSN the ordering lowers the transition temperature by about 25 °C [2], while in PST this temperature is raised by approximately 50 °C [1]. The ordering of the cations produces a doubling of the unit cell in all three ⟨100⟩ directions. Figure 1 shows the distribution of fully ordered cations on one of the {100} faces of the doubled cell.

$Pb(Fe_{0.5}Nb_{0.5})O_3$ (PFN) exists only in the disordered form [8, 9], with a broad transition to a ferroelectric state near 110–120 °C. Mössbauer spectra taken in both phases show very broad, quadrupole-split lines [10]. These indicate that the environment of the Fe nuclei is little changed by the onset of a reversible macroscopic polarization. Measurements of the heat capacity [11] gave a change in entropy at the transition of $0.92\ J\ K^{-1}\ mol^{-1}$, which is considerably smaller than would be expected if the atomic displacements were to go from a fully ordered to disordered arrangement at the transition. Recently the temperature and pressure dependence of the spontaneous

0953-8984/91/234173 + 13 $03.50

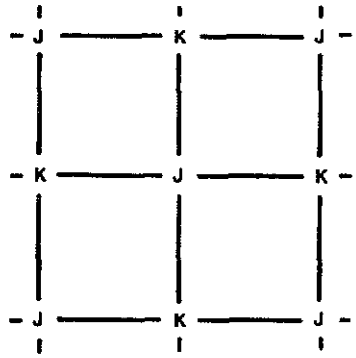

Figure 1. Distribution of distinguishable cation sites on {100} plane in fully ordered PSN.

polarization and permittivity have been reported [12, 13]. Hydrostatic pressure reduces the magnitude and temperature of the maximum in permittivity, but has little effect on the temperature dependence of the spontaneous polarization.

There is disagreement in the literature on the symmetry of ferroelectric PSN; [14] and [15] find a tetragonal distortion, while [3] reports rhombohedral symmetry with interaxial angle of 89.89(1)°. Rhombohedral symmetry for ferroelectric PFN was reported in [11], also with interaxial angle of 89.9°. A result of this extremely small distortion from cubic symmetry is that none of the lines in a powder diffraction pattern are resolved into multiple peaks. Locally the departures from cubic symmetry may be large, but an x-ray scattering experiment measures the averaged structure. Chemical disorder prevents development of long-range order in the atomic displacements, and so the resulting averaged structure is essentially cubic with each atomic site having a large Debye–Waller factor. The magnitude of this factor is the result of disorder in the displacements, not because of large vibrational amplitudes.

This paper describes x-ray and Mössbauer gamma ray scattering experiments performed on powders of PFN and PSN. The samples were prepared by well tried routes and characterized using x-ray diffraction. The diffractometer had good angular resolution of 0.08° FWHM in 2θ over most of the angular range studied. Monochromatic Cu $K\alpha_1$ radiation was employed. PFN was also studied using HRPD at SRS, Daresbury on line 9.1, where the resolution is approximately twice as good, yet none of the lines could be resolved into multiple peaks using this instrument either. However, evidence will be presented that the ferroelectric phase of PFN is tetragonal. A similar analysis for PSN was unable to assign a symmetry to the ferroelectric form because the linewidths showed near isotropic broadening.

Conventional Mössbauer absorption experiments were carried out on PFN confirming earlier findings [10]. Measurements of the intensity of Rayleigh-scattered Mössbauer gamma rays were made on all samples. The technique allows separation of elastic and inelastic scattering events, and hence enables Debye–Waller factors to be evaluated free from systematic error [16]. Phonon scattering peaks at reciprocal lattice points, and this scattering is included in the integrated intensity obtained with x-rays resulting in the magnitude of Debye–Waller factors being underestimated. No increase in inelastic scattering was detected near the phase transitions.

The magnitude and temperature dependence of vibrational amplitudes are conveniently described using an expansion of the one-particle potential [17]. Assuming that

the harmonic approximation is adequate, then

$$V(x, y, z) = V_0 + \tfrac{1}{2}\alpha(x^2 + y^2 + z^2)$$

where (x, y, z) are the displacements along $\langle 100 \rangle$ directions, and V_0 is a constant. The relationships between B, the Debye–Waller factor, α, and the mean square displacement $\langle u^2 \rangle$ are

$$B = 8\pi^2 k_B T/\alpha \qquad \langle u^2 \rangle = k_B T/\alpha.$$

Mair [18] found that the amplitudes of atomic displacements above displacive transitions in ordered perovskites can be adequately described within the harmonic approximation provided that α is allowed to be temperature dependent.

2. Samples preparation and characterization

2.1. Preparation

All samples were prepared from the relevant oxides; puratronic lead monoxide, ferric oxide and niobium pentoxide, and specpure scandium oxide, all obtained from Johnson Matthey Chemicals.

Suitable mixtures of the oxides were weighed out with an excess of 4% lead monoxide. These were ball milled under acetone for one hour, then fired at 800 °C for two hours, reground and ball milled, then refired at 1300 °C for one hour. Lead monoxide is lost during the firing process, and to minimize this, 20 g of lead zirconate were placed in a separate crucible in the furnace to provide an atmosphere rich in lead monoxide.

X-ray powder diffraction showed that PFN contained traces—about 3%—of a pyroclore phase which produced two weak lines with d spacings of 5.63 and 3.75 Å. For PSN, a weak line–less than 2% of the intensity of (110) reflection—was found with d spacing of 3.08 Å.

PSN was partially ordered by annealing the disordered sample at 950 °C for 40 days. To minimize loss of lead, a crucible containing lead zirconate was placed alongside the crucible containing PSN.

2.2. Characterization

2.2.1. A-site occupation. An estimate of the occupancy of the A-site for each sample was obtained from measurement of the integrated x-ray intensities of the first 12 fundamental powder diffraction lines at room temperature. Lines at higher angles were relatively weak because of the large Debye–Waller factors. The occupation probability was determined using a non-linear least squares analysis based on structure factors. For all models, suitably weighted scattering factors were calculated from parameters given in [19].

Several structures were assumed for the room temperature phases: the first placed lead at $(\frac{1}{2}, \frac{1}{2}, \frac{1}{2})$, atoms on B-sites at $(0, 0, 0)$ and oxygen at $(0, \frac{1}{2}, \frac{1}{2})$, $(\frac{1}{2}, 0, \frac{1}{2})$ and $(\frac{1}{2}, \frac{1}{2}, 0)$. Individual isotropic harmonic temperature factors were given to the three different sites, and the occupation probability of the A-site allowed to vary. These four parameters along with a scale factor were refined together. The results are given in table 1. The R-factor is defined as $\Sigma|F(\text{obs}) - F(\text{calc})|/\Sigma F(\text{obs})$.

Model 2 assumed rhombohedral symmetry. The magnitude of the displacements of A- and B-cations along [111] were around 0.2 Å. The refinement proceeded equally successfully with displacements of the same or opposite sign. The magnitudes of the temperature factors were less than for model 1 as one would have expected. The values

Table 1. Values of the isotropic coefficient in the harmonic potential for the three sites, occupation number for the A-site and *R*-factor.

	eV Å^{-2}				
Sample	(A)	(B)	(O)	p(A)	R
PFN	0.92 +/−0.22	1.45 +/−1.00	1.48 +/−2.19	0.82 +/−0.08	0.052
PSN (disordered)	0.80 +/−0.11	0.68 +/−0.20	0.46 +/−0.20	0.86 +/−0.06	0.044
PSN (ordered)	0.93 +/−0.03	1.09 +/−0.10	0.45 +/−0.06	0.91 +/−0.02	0.013

for p(A) were the same within the errors quoted in the table. Similar effects occurred when a tetragonal distortion was allowed, model 3. No statistically significant improvement in *R*-factor resulted with models 2 and 3, or when anisotropic temperatures were introduced into model 1.

The models were least satisfactory for PFN. A model was tried in which the parameter x in the formula $Pb_{1-x}(Fe_{0.5-x}Nb_{0.5+x})O_3$, which remains electrically neutral, was refined in addition to three independent Debye–Waller factors and scale factor, yet no improvement resulted.

2.2.2. Degree of order amongst B-cations in PSN. The ordering in PSN doubles the repeat distance in all three ⟨100⟩ directions, producing a face-centred cell. Figure 1 shows the distribution of fully ordered B-cations on one of the {100} faces of the enlarged cell.

If there were incomplete order, then on sites J and K of figure 1 the mean atomic scattering factors would become

$$\langle f(\mathrm{J})\rangle = rf(\mathrm{Sc}) + [1 - r]f(\mathrm{Nb}) \qquad \langle f(\mathrm{K})\rangle = rf(\mathrm{Nb}) + [1 - r]f(\mathrm{Sc})$$

where r is the long-range order parameter. The degree of order was estimated from the ratio of the intensity of (111) to (200) reflections when indexed on the doubled cell. Using the parameters obtained for model 1 described above gives a value for r of 0.90 ± 0.07.

2.2.3. Correlation length of long-range order parameter in PSN. The type of ordering of the cations in PSN will produce antiphase domains, where the sequence of alternating Nb and Sc cations along ⟨100⟩ directions is broken by two adjacent cations of the same type. It will be assumed that a break in periodicity only affects the B-cation sequence and not occupation probabilities or positions of the atoms. Antiphase domains broaden superlattice peaks without affecting the fundamental ones. When indexed on the doubled cell, superlattice peaks have indices that are all odd, while fundamental lines have indices that are all even.

The antiphase domain walls will be assumed to lie perpendicular to ⟨100⟩ directions and be independent of each other. The analysis follows closely that given in the book by Warren [20] (pp 216–26) for antiphase domains in $AuCu_3$. Provided the density of

Table 2. Integral breadths, widths and m values for (111), (200) and (311) reflections, indexed on the face-centred cell, obtained from fitting Pearson VII distributions to measured profiles.

$h_1h_2h_3$	Integral breadth/deg	FWHM/deg	m
1 1 1	161.34/262.2 = 0.62	0.47	1.45
2 0 0	785.54/5904.4 = 0.13	0.11	1.88
3 1 1	108.28/195.0 = 0.56	0.52	1.17

domain walls is not too large, the integral breadth, defined as (integrated intensity/peak intensity) is found to be

$$\beta(2\theta) \sim \lambda\gamma[h_1 + h_2 + h_3]/a_0 \cos\theta[h_1^2 + h_2^2 + h_3^2]^{1/2}$$

where λ is the x-ray wavelength, a_0 the lattice parameter, h_i Miller indices, and γ the probability of crossing an antiphase domain wall in passing from one of the planes depicted in figure 1 to an adjacent one.

The profiles of (111), (200) and (311) (doubled cell) were measured using a $\theta/2\theta$ step scan, and fitted with Pearson VII distributions. These are of the form

$$y(x) = y_0[1 + (x - \langle x\rangle)^2/ma^2]^{-m}$$

with width at height y_0/p given by

$$w(y_0/p) = 2a[m(p^{1/m} - 1)]^{1/2}.$$

The function varies from Lorentzian with $m = 1$ to Gaussian in the limit $m \to \infty$. Table 2 lists the results.

The reflections would have been fairly well represented by Lorentzians, so that assuming the width of (200) to be purely instrumental, then the contribution to the width of (111) from antiphase domains would be approximately $(0.47 - 0.11) = 0.36°$. Treating the integral breadths in the same way leads to an average distance of 208 Å between walls from (111) and 238 Å from (311) reflections, or, taking the mean, about 28 repeat distances of the large face-centred cell. This density is sufficiently low to make the approximations used above reasonable, i.e. $\gamma \ll 1$.

No evidence of ordering in PFN and un-annealed PSN was detected.

2.2.4. Symmetry of the three ferroelectric phases. $\theta/2\theta$ stepping scans through the first 12 fundamental reflections of the three samples at room temperature were performed using Cu $K\alpha_1$ radiation.

(i) *PFN.* None of the lines showed a measurable splitting into multiple peaks, although all lines were broadened. Each line could be fitted satisfactorily with a single Pearson VII distribution, and a Williamson–Hall plot of (FWHM $\times$ cos θ) versus sin θ is shown in figure 2(*a*). Experimental points are represented as circles, while squares give calculated values assuming a uniform tetragonal distortion of

$$a(\text{tetrag})/a(\text{cubic}) = 0.9995 \qquad c(\text{tetrag})/a(\text{cubic}) = 1.0010$$

after allowance for the angular resolution of the instrument, isotropic broadening, and a uniform strain broadening in addition to the effects of tetragonality. The calculated widths follow the same pattern as the experimentally determined values. The slope of a

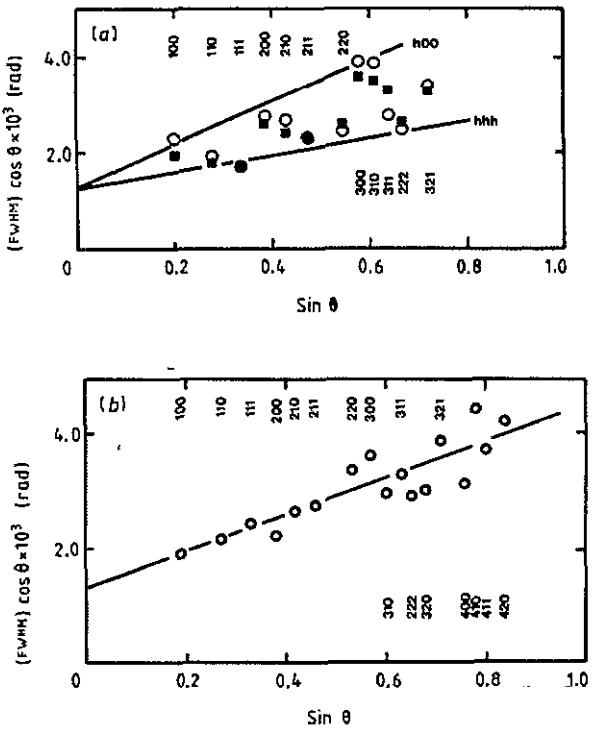

Figure 2. (*a*) Williamson–Hall plot for PFN at room temperature. Observations are depicted as open circles and calculated values as squares. Miller indices of reflections are given near the borders of the figure. The point for 300 represents two lines; 221 has the same Bragg angle. (*b*) Williamson–Hall plot using observed values of FWHM for ordered PSN at room temperature—disordered PSN values are the same within experimental error. Miller indices are given near the borders of the figure for each reflection. 221 has the same Bragg angle as 300; 330 the same as 411.

straight-line plot on the figure is a measure of strain broadening; the reciprocal of the intercept on the ordinate axis, size broadening. The indices refer to the small cell with lattice parameter ~4 Å.

If, as in $BaTiO_3$, the electrostrictive coefficients have magnitudes so that $Q_{11} \sim -2Q_{12}$, then {*hhh*} reflections would be unaffected by either a uniform or spatially varying tetragonal distortion, while reflections of the type {*h*00} would have the greatest widths. If the symmetry were rhombohedral, then {*h*00} would show the smallest widths and {*hhh*} the greatest. Two straight lines have been drawn through points representing {*h*00} and {*hhh*} reflections, and clearly the sample exhibits a tetragonal distortion.

(ii) *PSN*. Lines at room temperature from both ordered and disordered samples were broadened. Figure 2(*b*) shows a Williamson–Hall plot for ordered PSN; the widths for the disordered material showed nearly identical behaviour. Within the resolution of the experiment only an isotropic broadening was detectable, and so no allocation of symmetry was possible. The mean slopes and intercepts in the two figures are almost the same.

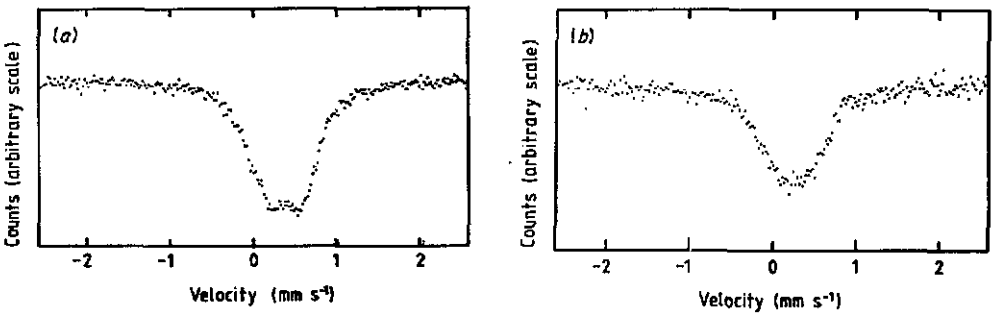

Figure 3. Mössbauer spectra of PFN at two temperatures obtained using ^{57}Co diffused into rhodium as a source of gamma rays. (*a*) PFN at 20 °C. (*b*) PFN at 142 °C.

3. Resonant absorption of Mössbauer gamma rays in PFN

In the main, the findings reported here confirm those reported earlier [10, 21]. The exception is the transition temperature reported in [10] as 155 °C, while in [21] it was given as 114 °C. The transition is broad, and from the scattering experiments discussed later, was in the range 110–125 °C.

Considerable difficulty was experienced in obtaining the spectra because of large photoelectric absorption. The thickness of the sample was approximately 10 mg cm^{-2} (0.02 mg cm^{-2} ^{57}Fe).

Two spectra are reproduced in figure 3, one above and one below the transition, clearly showing that the onset of a reversible, macroscopic polarization has little effect on the environment of ^{57}Fe nuclei. The isomer shift at room temperature is approximately 0.38 ± 0.02 mm s^{-1} (source ^{57}Co in Rh) compared with 0.52 ± 0.02 mm s^{-1} reported in [21] using ^{57}Co in stainless steel. These are consistent with each other and with iron being trivalent.

From the spectra one can estimate the relative strengths of Rayleigh and resonant scattering of Mössbauer gamma rays by PFN. A numerical estimate of the ratio

$$\int \sigma_S(\omega)\,\sigma_A(\omega)\,d\omega \Big/ \int \sigma_S(\omega)\,\sigma_S(\omega)\,d\omega$$

where $\sigma_A(\omega)$ is the cross section for resonant absorption of gamma rays by PFN and $\sigma_S(\omega)$ gives the energy distribution of gamma rays emitted by the source, gave the value of 0.16. The resonant scattering from PFN was calculated to be about 5% of the total Rayleigh scattering after allowing from thermal vibrations. This low fraction is the result of three factors: firstly the atomic scattering factor for lead is very large; secondly the absorption spectra in figure 3 are very broad compared with the natural linewidth of the source (about 0.1 mm s^{-1}); finally, there is a large isomer shift of 0.38 mm s^{-1}. The smallness of the resonant scattering means that it may be neglected compared with Rayleigh scattering, simplifying the analysis in section 5.

Resonant processes are slow, taking of the order of 10^{-7} s, the lifetime of the excited state of ^{57}Fe. Therefore the shape of the absorption spectra shown in figure 3 depends on the time-averaged position of the Fe nuclei, since 10^{-7} s is long compared with the reciprocal of phonon frequencies. In contrast, Rayleigh scattering is a rapid process; the

Table 3. Individual harmonic coefficients and occupation probability $p(A)$ for various temperatures.

Ordered PSN						
Temp (°C)	20	70	95	150	215	260
alpha(A)	0.93	0.81	0.79	0.80	0.85	0.97
alpha(B)	1.09	1.30	1.49	2.01	6.00	5.46
alpha(O)	0.45	0.79	0.78	1.79	2.13	2.46
$p(A)$	0.91	0.91	0.91	0.92	0.95	0.94
R-factor	0.013	0.032	0.035	0.033	0.025	0.030
Disordered PSN						
Temp (°C)	20	95	170	230	280	
alpha(A)	0.80	0.77	0.82	0.83	1.00	
alpha(B)	0.68	1.70	2.26	2.57	2.74	
alpha(O)	0.46	0.94	1.16	1.25	1.46	
$p(A)$	0.86	0.84	0.84	0.85	0.82	
R-factor	0.044	0.026	0.031	0.029	0.038	
PFN						
Temp (°C)	20	87	120	164	220	
alpha(A)	0.92	1.04	1.17	1.06	1.08	
alpha(B)	1.45	2.07	2.32	3.01	2.62	
alpha(O)	1.48	5.81	100	100	100	
$p(A)$	0.82	0.82	0.81	0.84	0.82	
R-factor	0.052	0.042	0.051	0.046	0.064	

intensity of Rayleigh-scattered gamma rays depends on the instantaneous position of all the atoms in the crystal.

4. Debye–Waller factors determined using x-rays

Integrated intensities of the first 12 fundamental reflections were measured at several temperatures for both ordered and disordered PSN and PFN, and individual values for α for each site, and occupation probability for the A-site were calculated. The results are given in table 3 and are discussed in section 6.

5. Debye–Waller factors determined using gamma rays

5.1. Technique of Rayleigh scattering of Mössbauer gamma rays

The source of gamma rays was ^{57}Co diffused into a foil of rhodium, 6 μm thick with other dimensions of 5×2 mm^2. The decay $^{57}\text{Co} \rightarrow {}^{57}\text{Fe}$ produces gamma rays with an energy of 14.4 keV, and about 70% of these are emitted without recoil. The 200 mCi source was held stationary and the radiation scattered by the stationary sample was passed through an absorber containing ^{57}Fe before detection. With the absorber also held stationary, nearly all gamma rays elastically scattered by the sample will be resonantly absorbed within the absorber, while gamma rays scattered with an energy change a little greater than the linewidth of the absorber will not be resonantly absorbed. By vibrating the absorber one can destroy all resonant absorption, and so using the difference in

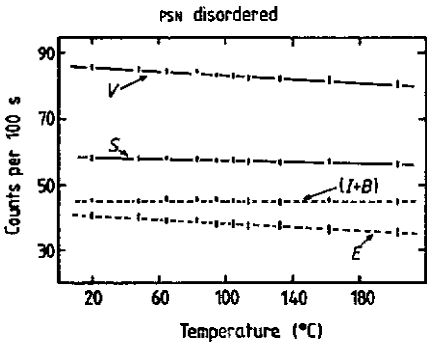

Figure 4. Counting rates of Rayleigh scattered gamma rays from disordered PSN as a function of temperature. Nomenclature: V, counting rate with absorber vibrating; S, counting rate with absorber held stationary; E, elastic counting rate derived from V and S; $(I + B)$, inelastic plus background counting rate equal to $(V - E)$. Phonon and Compton scattering are included in $(I + B)$.

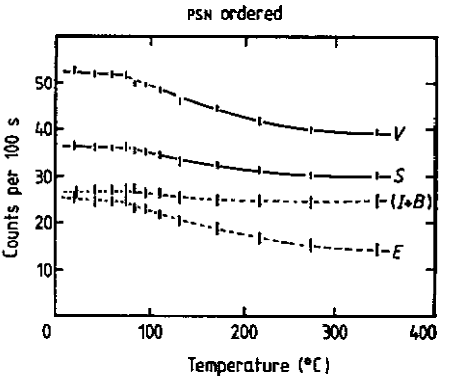

Figure 5. Counting rates of Rayleigh scattered gamma rays from ordered PSN as a function of temperature. Nomenclature: V, counting rate with absorber vibrating; S, counting rate with absorber held stationary; E, elastic counting rate derived from V and S; $(I + B)$, inelastic plus background counting rate equal to $(V - E)$. Phonon and Compton scattering are included in $(I + B)$.

counting rates obtained with stationary and moving absorbers the elastic and inelastic events may be separated. The energy resolution of the set-up depends upon the source–absorber combination: in the present case this was 8×10^{-8} eV. All radiation scattered with an energy change less than this was included with the true elastic scattering.

The source is weak when compared with the output of x-rays from the monochromator. Consequently poor angular resolution was used in order to increase the elastic count rate. This resulted in a large inelastic plus background count too, since most of the crystallites irradiated do not produce any elastic scattering.

The scattering from (110) reflection only for each sample was examined as a function of temperature; counts were accumulated over 24 hours at each temperature.

5.2. Results

The transition to the ferroelectric state in disordered and fully ordered PSN occurs at about 105 °C and 80 °C respectively [3]. Measurements of the counting rates with vibrating and stationary absorbers were taken as a function of temperature for both states, and the derived elastic and inelastic counting rates are shown in figures 4 and 5.

No evidence of the change to the ferroelectric state is apparent in the scattering from the disordered form—figure 4. For the ordered form, a distinct change occurs at about 80 °C, which is the transition temperature—figure 5. The positive curvature in the plot for temperatures above 80 °C was found for all reflections measured using x-rays, which indicates that the effect must be nearly isotropic. There is no significant increase in the inelastic scattering around the transition in either material.

The results for PFN are shown in figure 6; both elastic and inelastic counting rates show small discontinuities at the transition temperature. Measurements with x-rays also showed a dip in the temperature dependence of integrated intensity for reflections at

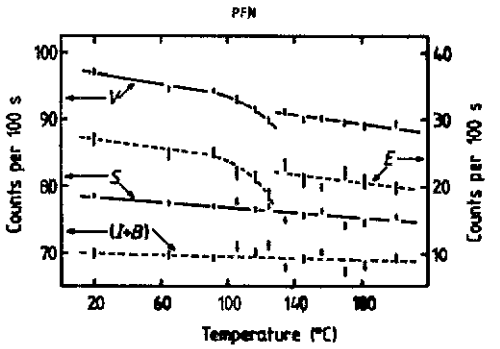

Figure 6. Counting rates of Rayleigh scattered gamma rays from PFN as a function of temperature. Nomenclature: V, counting rate with absorber vibrating; S, counting rate with absorber held stationary; E, elastic counting rate derived from V and S; $(I + B)$, inelastic plus background counting rate equal to $(V - E)$. Phonon and Compton scattering are included in $(I + B)$.

low Q-value (<3.8 Å^{-1}) as T_t was approached from below, while those at higher Q, for which the contribution from lead dominates, were more nearly monotonic.

6. Discussion

6.1. Changes in structure with temperature

The value of α for the A-site is effectively independent of temperature and the same magnitude for all three materials—the same value was found for PLZT [22]. At room temperature, α equal to 0.9 corresponds to a root mean square displacement of 0.17 Å.

The behaviour of the BO_6 octahedra is very similar to that in PLZT too. All materials show increasing octahedral distortion as temperature is lowered; i.e. T/α and hence $\langle u^2 \rangle^{1/2}$, increases with falling temperature. This is expected, since at room temperature, ferroelectricity is found, and is usually associated with off-centring of B-cations within the O_6 octahedra (although in a structural study of $Pb(Zr_{0.9}Ti_{0.1})O_3$, the displacement of lead was found to be bigger than that of the B-cations [23]). The exception to this behaviour is the B-site in PFN, for which T/α is roughly independent of temperature, although it has already been pointed out that the refinement for this material was not very satisfactory.

6.2. Magnitudes of temperature- and Q-dependent Debye–Waller factors obtained with x-rays and gamma rays

Phonon scattering peaks at reciprocal lattice points, and this scattering is included in the integrated intensity obtained with x-rays; the result is that the magnitudes of Debye–Waller factors are underestimated [16]. The energy discrimination of the gamma ray experiment allows separation of elastic from inelastic scattering leading to Debye–Waller factors free from this source of error.

A simple model is presented below which reproduces this effect and enables an estimate of the static and dynamic components of atomic displacements to be made.

The position of an atom in a disordered perovskite with effective overall cubic symmetry can be resolved into a time-dependent vibrational component, and a static displacement from the position it would occupy if the local symmetry were to be strictly cubic. One can write for the total displacement, t

$$t(t) = s + d(t).$$

Writing F_1 as the structure factor for the ideal, cubic perovskite, then to a reasonable approximation, the total scattering at a Bragg peak is given by

$$T(\text{total}) = E(\text{elastic}) + I(\text{inelastic}),$$

with

$$T = |F_1|^2 \exp - 2W_T[1 + (\boldsymbol{Q} \cdot \boldsymbol{d})^2]$$

where W_T is the overall Debye–Waller factor, namely

$$W_T = 8\pi^2 \sin^2\theta \langle t_Q^2 \rangle / \lambda^2.$$

t_Q is the component of the total displacement in the direction of the scattering vector. The first term gives the elastic scattering and the second term the first order inelastic scattering.

The gamma ray scattering experiment allows evaluation of W_T, but deriving a Debye–Waller factor from the total scattering measured in an x-ray scattering gives W_X, where

$$T = |F_1|^2 \exp - 2W_X$$

with

$$W_X \sim W_T - (\boldsymbol{Q} \cdot \boldsymbol{d})^2/2 = W_T - (Qd_Q)^2/2.$$

From W_T one obtains $\langle t_Q^2 \rangle$, and from $W_T - W_X$, $\langle d_Q^2 \rangle$. Assuming that there is no correlation between s and d, then

$$\langle t^2 \rangle = \langle s^2 \rangle + \langle d^2 \rangle$$

enabling $\langle s^2 \rangle$ to be found.

In fact, in this approximation, W_X gives $\langle s^2 \rangle$ directly. The assumptions made above are equivalent to adding all the inelastic scattering spread throughout the Brillouin zone to the x-ray integrated intensity. Values for $\langle s^2 \rangle$ deduced in this way are likely to be too big.

Plots of the log of the elastic intensity and the integrated x-ray intensity for (110) reflection versus temperature could be fitted adequately with straight lines and the results are given in table 4. The analysis is only appropriate for the ordered form of PSN below T_t, and the values given in the table are for the ferroelectric phase i.e. $T < 80$ °C. For PFN, temperatures in the range 90–125 °C were excluded from the plot. Values for the displacements obtained from these overall α are given in the table at 300 K. Their magnitude is largely determined by the heavy lead atom.

Included in the table are values for an overall α obtained from analyses of the first twelve fundamental reflections at room temperature for each sample. These are a little smaller than the values obtained from the temperature dependence of (110) reflection using x-rays. As the magnitude of Q increases, the approximation used above in writing the scattered amplitude as $F_1 \exp - W_X$ will become progressively worse, and is the likely source of this systematic trend.

Table 4. Values of the overall isotropic coefficient in the harmonic potential and root mean square displacement derived from gamma and x-ray scattering experiments.

	Overall alpha (eV Å^{-2})	RMS displacement at RT (Å)
Ordered PSN ($T < T_t$)		
Mössbauer $E(110)$ versus temp	0.7 ± 0.2	$\langle t^2\rangle^{1/2} = 0.19 \pm 0.04$
X-ray scattering $T(110)$ versus temp	0.9 ± 0.3	$\langle s^2\rangle^{1/2} = 0.17 \pm 0.04$
X-ray scattering 12 reflections RT	0.78 ± 0.13	$\langle s^2\rangle^{1/2} = 0.18 \pm 0.02$
Disordered PSN		
Mössbauer $E(110)$ versus temp	0.58 ± 0.13	$\langle t^2\rangle^{1/2} = 0.21 \pm 0.02$
X-ray scattering $T(110)$ versus temp	1.2 ± 0.2	$\langle s^2\rangle^{1/2} = 0.15 \pm 0.03$
X-ray scattering 12 reflections RT	0.81 ± 0.09	$\langle s^2\rangle^{1/2} = 0.18 \pm 0.01$
PFN		
Mössbauer $E(110)$ versus temp	0.25 ± 0.08	$\langle t^2\rangle^{1/2} = 0.32 \pm 0.04$
X-ray scattering $T(110)$ versus temp	1.2 ± 0.25	$\langle s^2\rangle^{1/2} = 0.15 \pm 0.03$
X-ray scattering 12 reflections RT	1.01 ± 0.19	$\langle s^2\rangle^{1/2} = 0.16 \pm 0.02$

PFN possesses the greatest disorder and differs from the other two materials in that a much larger part of the atomic displacement is dynamic. An inspection of figures 4, 5 and 6 shows that the inelastic and background counting rate was typically 70 per 100 s for PFN compared with about 45 for disordered PSN and around 25 for ordered PSN. The large counting rate for PFN is to be expected because of the large value of the dynamic component; one would expect greater scattering throughout the Brillouin zone. This suggests that the polarization direction in small parts of the sample is flipping between local minima in the free energy.

No evidence of a significant increase in inelastic scattering was found near T_t for any of the samples: soft-mode theory seems inappropriate to describe the transition in these disordered materials, including partially ordered PSN.

Acknowledgments

I wish to thank the Science and Engineering Council for financial support.

References

[1] Setter N and Cross L E 1980 *J. Appl. Phys.* **51** 4356
[2] Stenger C G F and Burggraff A J 1980 *Phys. Status Solidi* a **61** 275

[3] Stenger C G F and Burggraaf A J 1980 *Phys. Status Solidi* a **61** 653
[4] Randall C A, Barber D J, Whatmore R W and Groves P 1986 *J. Mater. Sci.* **21** 4456
[5] Cross L E 1987 *Ferroelectrics* **76** 241
[6] Salje E and Bismayer U 1989 *J. Phys.: Condens. Matter* **1** 6967
[7] Bismayer U, Devaraajan V and Salje E 1989 *J. Phys.: Condens. Matter* **1** 6977
[8] Drabkin G M, Mal'tsev E I and Plaktii V P 1965 *Sov. Phys.–Solid State* **7** 997
[9] Roginskaga Yu E, Venevtsev Yu N and Zhdanou G S 1965 *Sov. Phys.–JETP* **21** 817
[10] Bell R O 1968 *J. Phys. Chem. Solids* **29** 1
[11] Bhat K C, Keer H V and Biswas A B 1974 *J. Phys. D: Appl. Phys.* **7** 2077
[12] Yasuda N and Ueda Y 1989 *J. Phys.: Condens. Matter* **1** 497
[13] Yasuda N and Ueda Y 1989 *J. Phys.: Condens. Matter* **1** 5179
[14] Ismailzade I G 1959 *Sov. Phys. (Cryst.)* **4** 289
[15] Kuchar F and Valenta M W 1971 *Phys. Status Solidi* a **6** 525
[16] O'Connor D A 1972 *Perspectives in Mössbauer Spectroscopy* (New York: Plenum)
[17] Willis B T M and Prior A W 1975 *Thermal Vibrations in Crystallography* (Cambridge: Cambridge University Press)
[18] Mair S L 1982 *Acta Crystallogr.* A **38** 790
[19] Cromer D T and Mann J B 1968 *Acta Crystallogr.* A **24** 321
[20] Warren B E 1969 *X-ray Diffraction* (Reading, MA: Addison-Wesley)
[21] Sklyarevskii V V, Lukashevich I I, Romanov V P, Filippov N I, Venevtsev Yu N and Viskov A S 1966 *JETP Lett.* **3** 135
[22] Darlington C N W 1989 *Phys. Status Solidi* a **113** 63
[23] Glazer A M, Mabud S A and Clarke R 1978 *Acta Crystallogr.* B **34** 1060